Microwave Device Inspired by Fiber-Optic Extrinsic Fabry-Perot Interferometer: A Novel Ultra-Sensitive Sensing Platform

Chen Zhu, *Student Member, IEEE*, Rex E. Gerald, and Jie Huang, *Member, IEEE*

***Abstract*—The fiber-optic extrinsic Fabry–Perot interferometer (EFPI) is one of the simplest sensing configurations and is widely used in various applications. Inspired by the EFPI, we report a novel and universal ultra-sensitive microwave sensing platform based on an open-ended hollow coaxial cable resonator. Two highly-reflective microwave reflectors were fabricated in a coaxial cable to form a microwave Fabry–Perot etalon. Although the operating wavelength of the proposed device is increased by five orders of magnitude compared to the fiber-optic EFPI (e.g., from 1500 nm to 150 mm), the resolution regarding the "*pseudo* cavity length" of the proposed device is as high as 0.6 nanometer, which is comparable to that of the EFPI. The resolution can be further increased by high-precision machining of the device. Due to its low cost, high sensitivity, all-metal structure, robustness, and ease of signal demodulation, it is envisioned that the proposed device will revolutionize the sensing field and enable many important sensing applications that take place in harsh environments.**

***Index Terms*—Displacement, extrinsic Fabry–Perot interferometer, fiber-optic sensor, microwave device, open-ended coaxial cable resonator.**

I. Introduction

FIBER-OPTIC extrinsic Fabry-Perot interferometers (EFPIs) have been used for sensing a myriad of measurable variables, including displacement [1], acoustic frequency/pressure [2], static pressure [3], strain [4], sliding and debonding [5], acceleration [6], and inclination [7]. A typical EFPI is constructed using an unmodified telecommunication single-mode fiber (SMF) and an external reflector that is placed a certain distance (e.g., tens of micrometers to a few millimeters) away from the cleaved end facet of the fiber. A Fabry-Perot cavity is formed between the optical fiber endface and the external reflector. When broadband probing light is used to illuminate the Fabry-Perot cavity, the two reflected light beams from the two reflectors interfere and generate a fringe pattern in the spectral domain. The fringe pattern is defined by the phase delay of the cavity, which is determined by the cavity length and the refractive index of the cavity medium [8]. Therefore, in general, physical or chemical measurable variables that can be correlated to either the cavity length or the refractive index of the cavity medium can be measured using the EFPI configuration. Compared with other fiber-optic interferometric sensors, the EFPI offers unique advantages, including ease of fabrication, high sensitivity, high resolution, compactness, and high structural flexibility. However, to ensure a stable and high-quality interference signal, SMFs are typically employed to construct EFPI sensors, which essentially limits the application scope of EFPI sensors [9]. For instance, SMFs are made of fused silica, which is not stable at extremely high temperatures (e.g., $>$1000 °C). Therefore, high-temperature applications of EFPI sensors are hindered. Additionally, accurate interrogation and demodulation of an EFPI sensor are relatively difficult to achieve, requiring a broadband light source, a high-precision spectrometer, and sophisticated algorithms.

A coaxial cable is also a type of single-mode transmission line, operating in radiofrequency (RF) regime, that has been commonly used for communication applications. Governed by the same fundamental physics, researchers strived in recent years to translate several fiber-optic sensing configurations to coaxial cables, including the fiber Bragg grating [10] and the Fabry-Perot interferometer [11]. The resultant coaxial cable Bragg grating and the coaxial cable Fabry-Perot interferometer were demonstrated for sensing strain up to 5% [12], which is approximately five times larger than the maximum strain measured by traditional fiber-optic sensors. Very recently, we proposed and demonstrated a new sensing structure, the hollow coaxial cable Fabry-Perot resonator (HCC-FRP), inspired by the Fabry-Perot etalon [13]–[17]. The all-metal design of the HCC-FPR greatly improves its thermal stability and tolerance, which is expected to provide an alternative to fiber-optic counterparts for extremely high-temperature sensing applications. However, the existing coaxial cable in-line sensor devices suffered from low measurement resolution due to the long interrogation wavelength, approximately two orders of magnitude lower resolution than that typically encountered for fiber-optic sensors. Additionally, the structural design flexibility of HCC-FRP devices is limited due to the in-line structure.

In this paper, we report our innovative work on a novel microwave device, a universal ultra-sensitive sensing platform,

Manuscript received June 16, 2020; revised July 27, 2020 and August 12, 2020; accepted August 17, 2020. Date of publication August 20, 2020; date of current version December 15, 2020. This work was supported in part by the NSF under Award 2027571, in part by the Leonard Wood Institute in cooperation with the U.S. Army Research Laboratory, and in part by the Cooperative Agreement under Grant W911NF-14-2-0034. *(Corresponding author: Jie Huang.)*

The authors are with the Department of Electrical and Computer Engineering, Missouri University of Science and Technology, Rolla, MO 65409 USA (e-mail: cznwq@mst.edu; rexgeraldii@gmail.com; jieh@mst.edu).

Color versions of one or more of the figures in this article are available online at https://ieeexplore.ieee.org.

Digital Object Identifier 10.1109/JLT.2020.3018380

0733-8724 © 2020 IEEE. Personal use is permitted, but republication/redistribution requires IEEE permission.
See https://www.ieee.org/publications/rights/index.html for more information.

Authorized licensed use limited to: Missouri University of Science and Technology. Downloaded on May 29,2021 at 22:40:03 UTC from IEEE Xplore. Restrictions apply.

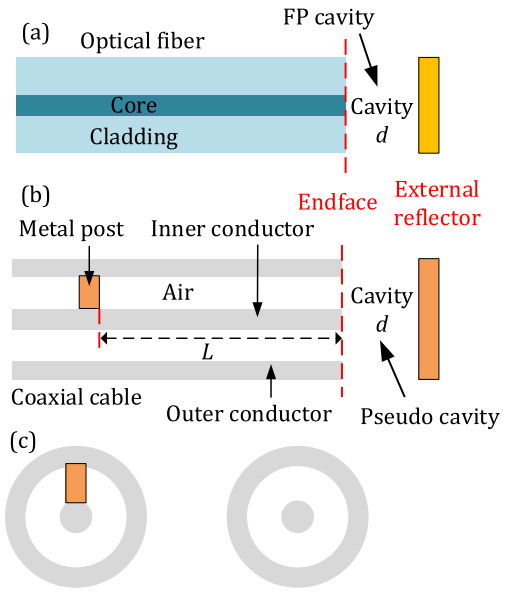

Fig. 1. Structural comparison between the fiber-optic EFPI and the "coaxial cable EFPI" or OE-HCCR. (a) Schematic of a typical fiber-optic EFPI. (b) Schematic of the proposed OE-HCCR. L denotes the length of the Fabry-Perot cavity. (c) Cross-section views of the two microwave reflectors used in the OE-HCCR. Figures of the fiber-optic EFPI and the OE-HCCR device are not drawn to scale.

which was motivated by the fiber-optic EFPI. The fundamental physics of the device, named the open-ended hollow coaxial cable resonator (OE-HCCR), is discussed. Numerical calculations were performed to predict the performance of the novel device. A prototype device was fabricated and tested to verify the proposed technique.

II. Principle of OE-HCCR

Schematic drawings of a fiber-optic EFPI and the proposed OE-HCCR with air cavities are shown in Fig. 1. The Fabry-Perot cavity of the EFPI is formed between the endface of the optical fiber and the external reflector. According to two-beam interference theory, the phase-matching condition of the fiber-optic EFPI where destructive interference occurs is given by [18]

$$\frac{4\pi d}{\lambda} + \pi = 2\mathrm{m}\pi + \pi, \tag{1}$$

where λ is the wavelength; d is the Fabry-Perot (FP) cavity length indicated in Fig. 1(a); and, m is an integer denoting the resonance order. The resonance wavelengths are then given by

$$\lambda = \frac{2}{m}d. \tag{2}$$

Therefore, by tracking the shifts of the resonance wavelength, changes in the cavity length of the EFPI sensor caused by changes in measurands (e.g., displacement, pressure, etc.) can be determined. The wavelength-tracking method provides high measurement resolution and accuracy, while the dynamic range is limited due to the periodic interference pattern. Mimicking the fiber-optic EFPI, we propose a "coaxial cable EFPI" (i.e., OE-HCCR) that can be used as a novel ultra-sensitive sensing platform. Fig. 1(b) presents a schematic of the proposed configuration. Different from the fiber-optic EFPI, the Fabry-Perot cavity is formed by the metal post reflector and the endface reflector of the coaxial cable. The metal post connects the concentric conductors, creating a short circuit, thus serving as the first microwave reflector. The endface of the coaxial cable is an open circuit, acting as the second microwave reflector. Fig. 1(c) shows the cross-section views of the two reflectors. The reflection spectrum of the cavity resonator is given by [15]

$$S = \sqrt{\frac{{r_1}^2 - 2r_1r_2\cos(4\pi L/\lambda - \varphi_1 - \varphi_2) + {r_2}^2}{1 - 2r_1r_2\cos(4\pi L/\lambda - \varphi_1 - \varphi_2) + {r_1}^2{r_2}^2}}, \tag{3}$$

where φ_1 and φ_2 represent the phase terms of the two microwave reflectors; r_1 and r_2 represent the magnitude terms of the two microwave reflectors; and, L is the length of the Fabry-Perot cavity. The phase-matching condition of the OE-HCCR is given by

$$\frac{4\pi L}{\lambda} - \varphi_1 - \varphi_2 = 2m\pi, \tag{4}$$

Thus, the resonance frequencies of the cavity are given by

$$f = \frac{c(2m\pi + \varphi_1 + \varphi_2)}{4\pi L}. \tag{5}$$

Note that the *pseudo* cavity of the OE-HCCR device with a length of d indicated in Fig. 1(b), i.e., the gap between the endface of the coaxial cable and the external reflector, is not the Fabry-Perot cavity, which is the major difference between the fiber-optic EFPI and OE-HCCR device. However, the operating principle for the EFPI and OE-HCCR as a sensor device is the same, where measurands of interest are encoded into the movement (deflection) of the external reflector, as discussed below.

Importantly, the phase term associated with the second reflector of the OE-HCCR device (i.e., φ_2, the endface) strongly depends on the *pseudo* cavity length d, which is the fundamental basis of the proposed configuration as a sensing platform. According to transmission line theory, the complex reflectivity of the endface reflector is given by

$$r_2 e^{j\varphi_2} = \frac{Z - Z_0}{Z + Z_0} = \frac{1/j2\pi fC - Z_0}{1/j2\pi fC + Z_0}, \tag{6}$$

where Z and Z_0 denote the impedance of the endface reflector and the characteristic impedance of the coaxial cable, respectively; and, C is the total capacitance over the enface aperture of the OE-HCCR. As the *pseudo* cavity length d decreases, the capacitance C of the cavity increases exponentially [19], [20]. According to Eq. (6), the increase in the capacitance decreases the phase term associates with the endface reflector, thus reducing the resonance frequency of the device (see Eq. (5)). The external reflector of the OE-HCCR should be made of conducting material such as metal to obtain the greatest dependency of the resonance frequency on the length of the *pseudo* cavity. The surface of the external reflector can be rough and not optically-reflective, which differs from the reflector for the fiber-optic EFPI.

Authorized licensed use limited to: Missouri University of Science and Technology. Downloaded on May 29,2021 at 22:40:03 UTC from IEEE Xplore. Restrictions apply.

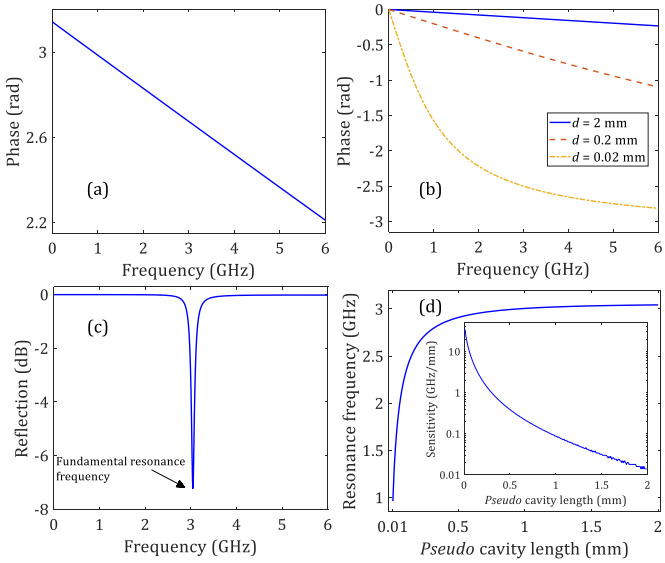

Fig. 2. Numerical investigations of the proposed OE-HCCR device. (a) Simulated phase term of the metal post as a function of frequency. (b) Calculated phase term of the endface reflector as a function of frequency for different settings of the *pseudo* cavity length. (c) An example of the reflection spectrum, where the fundamental resonance frequency of the OE-HCCR is approximately 3 GHz. (d) Theoretically-predicted dependence of the fundamental resonance frequency of the OE-HCCR device on the *pseudo* cavity length. The inset is a plot of the predicted sensitivity (the derivative of the fundamental resonance frequency with respect to the *pseudo* cavity length, on a log scale) as a function of the *pseudo* cavity length.

The size dimensions of the coaxial cable should be carefully determined to avoid an impedance mismatch at the signal input end of the device and to ensure a high-quality resonance pattern from the OE-HCCR. The characteristic impedance of the hollow coaxial cable is given by [21]

$$Z_0 \approx 138 \cdot \log_{10} \frac{b}{a}, \tag{7}$$

where a and b are the radii of the inner and outer conductors, respectively. The prototype OE-HCCR was designed with a and b equal to 1.10 mm and 2.50 mm, respectively, so that the characteristic impedance of the hollow coaxial cable would be approximately 50 Ohms, a typical value for commonly used commercial coaxial cables. Additionally, the selected size dimensions also enable the hollow coaxial cable to be easily connected to a standard SubMiniature version A (SMA) female connector. Numerical calculations were first performed to investigate the response of the OE-HCCR to variations of the *pseudo* cavity length. The numerical results are presented in Fig. 2. Note that both the phase terms of the two microwave reflectors are a function of frequency, and thereby Eq. (5) has no analytical solution. We first employed full-wave simulations (ANSYS HFSS) to obtain the reflection coefficient of the metal post (i.e., r_1 and φ_1). The reflection coefficient of the endface reflector (i.e., r_2 and φ_2) was calculated based on Eq. (6), where the capacitance C was determined via static analyses [19]. Figs. 2(a) and (b) show the calculated phase terms of the two microwave reflectors. The phase term associated with the endface reflector decreased as the *pseudo* cavity length decreased. Plugging in the solved reflection coefficients of the two reflectors into Eq. (3), the spectrum of the cavity resonator can be obtained, through which the resonance frequency of the cavity can be determined. The reflection spectrum of the device where the *pseudo* cavity length was set to 2 mm is plotted in Fig. 2(c). The diameter of the metal post and the distance between the metal post and the endface were set to 1.50 mm and 20.0 mm in the calculation, respectively. In the frequency observation bandwidth from 0 to 6 GHz, only one resonance dip was observed, corresponding to the fundamental resonance frequency. Note that the frequency can be tuned by adjusting the length of the Fabry-Perot cavity L, according to Eq. (5). The dependence of the fundamental resonance frequency on the *pseudo* cavity length d is shown in Fig. 2(d). The resonance frequency decreased exponentially as the *pseudo* cavity length decreased, demonstrating the high sensitivity of the OE-HCCR device to variations of the *pseudo* cavity length. More importantly, the sensitivity of the resonance frequency to the *pseudo* cavity length increased exponentially as the *pseudo* cavity length decreased, as shown in the inset of Fig. 2(d). As the *pseudo* cavity length decreased to 0.30 mm, the sensitivity increased to 1 GHz/mm; as the *pseudo* cavity length further decreased to 0.05 mm, the sensitivity reached 11 GHz/mm.

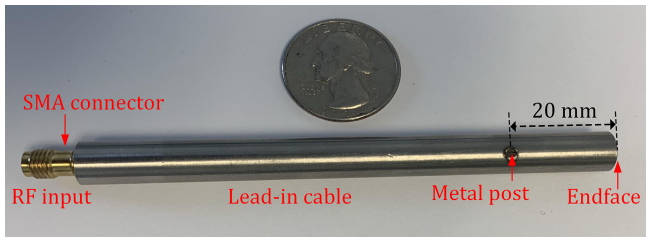

Fig. 3. Photograph of a prototype OE-HCCR device.

III. Result

A prototype device was fabricated using stainless steel, as shown in Fig. 3. Note that fabrication of the prototype OE-HCCR device only involved traditional metal welding and cutting procedures, which are low-cost processes. The all-metal structure also provides high mechanical robustness and improves the high-temperature tolerance of the device. The OE-HCCR device works in a convenient reflection mode. An SMA female connector was connected to the back end of the OE-HCCR device and used as the RF signal input connector. A portable vector network analyzer (VNA, Anritsu 46121B) was employed to make reflection measurements, serving as the microwave source and the detector. A conducting plate (made of stainless steel) was mounted on a translation stage, and carefully positioned to adjust the *pseudo* cavity length (i.e., the gap distance) of the OE-HCCR device.

Fig. 4 presents the experimental results used to characterize the performance of the prototype OE-HCCR device. The measured reflection spectrum of the OE-HCCR device, when the *pseudo* cavity length was approximately 2 mm (measured using a caliper), is plotted in Fig. 4(a). A resonance dip at

Authorized licensed use limited to: Missouri University of Science and Technology. Downloaded on May 29,2021 at 22:40:03 UTC from IEEE Xplore. Restrictions apply.

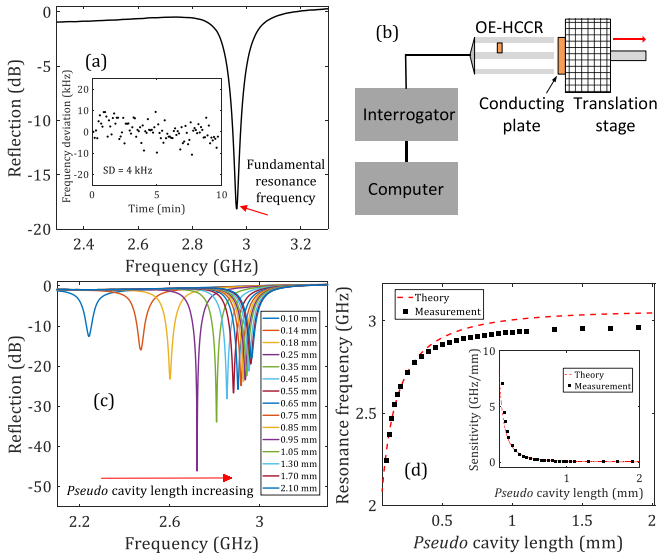

Fig. 4. Experimental results used to characterize the performance of the prototype OE-HCCR device. (a) Measured reflection spectrum of the OE-HCCR device. The inset shows the deviation of the measured resonance frequency of the device over a time period of 10 min when the *pseudo* cavity length was kept constant. (b) Experimental setup used to test the response of the OE-HCCR device at various settings of the *pseudo* cavity length. (c) Measured reflection spectra of the OE-HCCR device for different settings of the *pseudo* cavity lengths. (d) Measured and theoretically-predicted relationships between the resonance frequency of the OE-HCCR device and the *pseudo* cavity length. The inset shows the measured and theoretically-predicted sensitivity of the OE-HCCR device as a function of the *pseudo* cavity length.

around 2.964 GHz was obtained, which is close to the theoretical prediction of 3.043 GHz (see Fig. 2(c)). Fig. 4(b) illustrates the experimental setup used to characterize the performance of the OE-HCCR device. As the translation stage moved away from the endface of the OE-HCCR device, the *pseudo* cavity length increased. The measured reflection spectra of the OE-HCCR device for different settings of the *pseudo* cavity lengths are shown in Fig. 4(c). Note that the initial *pseudo* cavity length was set to be as small as possible through visual inspection. However, due to machining errors, the endfaces of the inner conductor and the outer conductor were offset by approximately 0.10 mm (measured using a caliper). Therefore, the initial *pseudo* cavity length was estimated to be 0.10 mm. As the *pseudo* cavity length increased, the resonance dip shifted to the high-frequency region, as expected. Note that the evolution of the resonance depth of the reflection spectrum is a result of the frequency-dependence of the reflectivity of the metal post. Fig. 4(d) shows the measured resonance frequency of the OE-HCCR device as a function of the *pseudo* cavity length. The inset shows the measured sensitivity of the OE-HCCR device (change in resonance frequency/change in the *pseudo* cavity length) as a function of the *pseudo* cavity length. The theoretical predictions shown in the inset of Fig. 2(d) are also included in Fig. 4(d) for comparison. The resonance frequency of the OE-HCCR device increased as the *pseudo* cavity length increased; the sensitivity decreased exponentially as the *pseudo* cavity length increased. The overall trends of the measurement and theoretical prediction results matched well. The measured sensitivity reached 1 GHz/mm when the *pseudo* cavity length was set to 0.3 mm. The experimentally achieved highest sensitivity using the prototype OE-HCCR device was 7 GHz/mm. The stability of the device was experimentally quantified by continuously recording the reflection spectrum for 10 min when the *pseudo* cavity length was set to 2 mm. The standard deviation (SD) of the resonance frequency was determined to be 4 kHz, as shown in the inset of Fig. 4(a). Therefore, the resolution of the OE-HCCR device was estimated to be 4 nm over a range of 0-0.3 mm and 0.6 nm over a range of 0-0.11 mm. Note that as reported in our previous work [15], the displacement resolution of a traditional HCC-FPR was approximately 10 μm over a sub-meter dynamic range. The obtained resolution of the OE-HCCR is at least three orders of magnitude greater than that of the traditional HCC-FPR, although the dynamic range is sacrificed. This significant improvement in measurement resolution is fundamentally due to the novel sensing scheme of the OE-HCCR, where the phase term φ_2 associated with the endface reflector exhibits an exponential dependence on the *pseudo* cavity length (i.e., displacement of the external conducting plate). A fundamental comparison between the HCC-FPR and the OE-HCCR is shown in the subsequent Discussion section.

IV. Discussion

Both the theoretical predictions and experimental results demonstrate the ultra-high sensitivity of the OE-HCCR device to variations of the *pseudo* cavity length. Compared to a fiber-optic EFPI, the resolution of the OE-HCCR device is of the same order of magnitude, namely 4 nm over a small dynamic range (0-0.3 mm). However, the discrete resonance pattern of the OE-HCCR device makes it easier to monitor parameters of interest (e.g., displacement) by simply tracking the resonance frequency. The system cost of the OE-HCCR device is much lower than a fiber-optic EFPI system, including sensor fabrication and the interrogation unit. Note that although a VNA was employed in the demonstration, a less expensive scalar network analyzer can be used to interrogate the OE-HCCR device. The ruggedized all-metal structure of the OE-HCCR device offers high mechanical stability, robustness, and drastically enhanced temperature tolerances, making the OE-HCCR device an excellent candidate for high-temperature applications. Conducting materials with higher melting points (e.g., tungsten, graphite) can be used to construct the OE-HCCR device for applications at extremely high temperatures. Although the size of the first prototype OE-HCCR device was approximately 50 times larger than a bare optical fiber with a cladding diameter of 125 μm, the dimensional size of the OE-HCCR device can be further reduced to the micrometer scale according to transmission line theory. One major limitation of the OE-HCCR device is its susceptibility to electromagnetic interference (EMI). The device should be carefully packaged in a metal container (Faraday cage) to avoid EMI in harsh environments. However, the packaging could increase the size and weight of the OE-HCCR device. Therefore, it is preferable to use the proposed OE-HCCR device in EMI-free harsh environments that experience high temperatures, high pressures, and that involve heavy-duty circumstances.

Authorized licensed use limited to: Missouri University of Science and Technology. Downloaded on May 29,2021 at 22:40:03 UTC from IEEE Xplore. Restrictions apply.

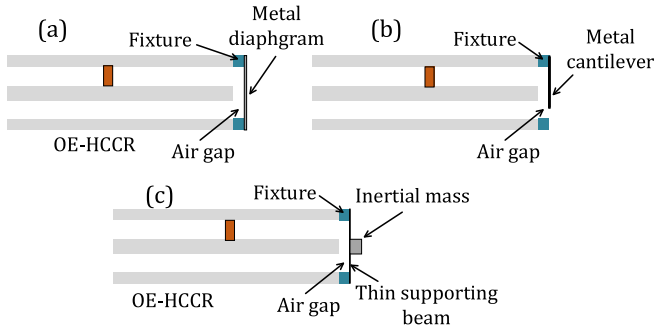

Fig. 5. Examples of sensors that can be fabricated based on the OE-HCCR device. (a) A pressures sensor. (b) An acoustic sensor. (c) An accelerometer.

In previously reported HCC-FPR sensing devices, variations of the measurand of interest (e.g., displacement, liquid level, etc.) were encoded into changes in the cavity length of the cavity resonator (i.e., L) [14], [15], leading to changes in the phase delay of the resonator. The resultant variations of the phase delay were linearly proportional to variations of the cavity length L. In the present work, the proposed OE-HCCR operates based on a novel sensing scheme, where variations of the measurand of interest (e.g., displacement) are correlated to changes in the *pseudo* cavity length of the OE-HCCR, i.e., changes in the phase term φ_2 associated with the endface reflector of the resonator. The changes in φ_2 modify the total phase delay of the cavity resonator (see Eqs. (4) and (5)) and manifest as shifts in the resonance frequency. Importantly, the phase term φ_2 exhibits an exponential dependence on the *pseudo* cavity length of the OE-HCCR due to the significantly concentrated fringing electric field in the gap between the endface of the coaxial cable and the external conducting plate. As the *pseudo* cavity length decreases, the capacitance associated with the endface aperture increases exponentially, resulting in an exponential decrease in the phase term φ_2. An intuitive explanation of this exponential dependence is the transition of the endface reflector from an open circuit to a short circuit as the conducting plate approaches the endface of the coaxial cable and eventually contacts the endface. As a result, compared to the HCC-FPR, the measurement sensitivity of the OE-HCCR was significantly improved by three orders of magnitude. Moreover, the extrinsic configuration of the OE-HCCR opens up new avenues for developing a new generation of ultra-sensitive microwave sensor devices with unique features and comparable sensitivities to fiber-optic counterparts.

We envision that couplings of the metal conductor to the open end of the OE-HCCR device, using judicious mechanical designs, will produce flexibly-designed sensor devices capable of measurements of a variety of physical parameters, such as temperature, acoustic pressure, static pressure, vibration, acceleration, and tilt with high sensitivity. Fig. 5 includes schematic diagrams of several examples of sensors that can be fabricated using the OE-HCCR device platform, mimicking the well-known fiber-optic EFPI sensors. For example, an OE-HCCR device configured as a pressure sensor can be fabricated by replacing the metal plate with a metal diaphragm that deflects when it is subject to variations of static or dynamic pressures, as illustrated in Fig. 5(a). Alternatively, a metal cantilever can be fabricated on the enface of the OE-HCCR device so that it can be used for acoustic sensing, as shown in Fig. 5(b). Fig. 5(c) illustrates an OE-HCCR device vibration sensor or accelerometer, where an inertial mass block is employed as part of the vibration responsive element. Note that all these sensors can be used at elevated temperatures due to the all-metal structures. On the other hand, the OE-HCCR device is also sensitive to the permittivity of the medium in the *pseudo* cavity (the gap between the endface and the external reflector), similar to the fiber-optic EFPI. The permittivity sensitivity also increases as the *pseudo* cavity length decreases. Therefore, the proposed OE-HCCR device is also a chemical sensing platform. By including functional materials (e.g., metal-organic framework, zeolite, etc.) in the gap between the open end and the metal reflector, the OE-HCCR device can be configured as various ultra-sensitive chemical sensors [22]. Another unique and striking feature of the OE-HCCR device is that the phase information of the device can be directly measured in the microwave domain. By combining a phase-shift amplification technique, it is possible to resolve changes in the *pseudo* cavity length of the OE-HCCR device with picometer resolution [23].

V. Conclusion

To summarize, we invented, fabricated, and tested a novel sensing platform that is based on a microwave resonator. The idea of the OE-HCCR device originates from the well-known fiber-optic EFPI. The resonance frequency of the OE-HCCR device strongly depends on the *pseudo* cavity length of the device (i.e., the air gap in front of the open end), exhibiting a resolution of as high as 0.6 nm. The OE-HCCR device can be used as a sensor with ultrahigh sensitivity by encoding measurands of interest into the *pseudo* cavity length. We envision that the proposed general OE-HCCR device platform will provide an uncharted route to a novel generation of low-cost and ultra-sensitive sensors that operate at a low frequency (sub-gigahertz and gigahertz regimes) for measuring a variety of physical quantities required by many applications.

Acknowledgment

The views and conclusions contained in this document are those of the authors and should not be interpreted as representing the official policies, either expressed or implied, of the Leonard Wood Institute, the Army Research Laboratory or the U.S. Government. The U.S. Government is authorized to reproduce and distribute reprints for Government purposes notwithstanding any copyright notation hereon.

References

[1] M. Schmidt, B. Werther, N. Fürstenau, M. Matthias, and T. Melz, "Fiber-optic extrinsic Fabry–Perot interferometer strain sensor with< 50 pm displacement resolution using three-wavelength digital phase demodulation," *Opt. Express*, vol. 8, no. 8, pp. 475–480, 2001.

[2] R. Nuster *et al.*, "Downstream Fabry–Perot interferometer for acoustic wave monitoring in photoacoustic tomography," *Opt. Lett.*, vol. 36, no. 6, pp. 981–983, 2011.

Authorized licensed use limited to: Missouri University of Science and Technology. Downloaded on May 29,2021 at 22:40:03 UTC from IEEE Xplore. Restrictions apply.

[3] F. Guo, T. Fink, M. Han, L. Koester, J. Turner, and J. Huang, "High-sensitivity, high-frequency extrinsic Fabry–Perot interferometric fiber-tip sensor based on a thin silver diaphragm," *Opt. Lett.*, vol. 37, no. 9, pp. 1505–1507, 2012.
[4] Y. Huang, T. Wei, Z. Zhou, Y. Zhang, G. Chen, and H. Xiao, "An extrinsic Fabry–Perot interferometer-based large strain sensor with high resolution," *Meas. Sci. Technol.*, vol. 21, no. 10, 2010, Art. no. 105308.
[5] C. Zhu *et al.*, "An optical interferometric triaxial displacement sensor for structural health monitoring: Characterization of sliding and debonding for a delamination process," *Sensors*, vol. 17, no. 11, 2017, Art. no. 2696.
[6] F. Bruno, M. Pisco, G. Gruca, N. Rijnveld, and A. Cusano, "Opto-mechanical lab-on-fiber accelerometers," *J. Lightw. Technol.*, vol. 38, no. 7, pp. 1998–2009, Apr. 2020.
[7] Y. Zhuang, Y. Chen, C. Zhu, R. E. Gerald, and J. Huang, "Probing changes in tilt angle with 20 nanoradian resolution using an extrinsic Fabry–Perot interferometer-based optical fiber inclinometer," *Opt. Express*, vol. 26, no. 3, pp. 2546–2556, 2018.
[8] M. Islam, M. M. Ali, M.-H. Lai, K.-S. Lim, and H. Ahmad, "Chronology of Fabry–Perot interferometer fiber-optic sensors and their applications: A review," *Sensors*, vol. 14, no. 4, pp. 7451–7488, 2014.
[9] M. Han and A. Wang, "Exact analysis of low-finesse multimode fiber extrinsic Fabry–Perot interferometers," *Appl. Opt.*, vol. 43, no. 24, pp. 4659–4666, 2004.
[10] T. Wei, S. Wu, J. Huang, H. Xiao, and J. Fan, "Coaxial cable Bragg grating," *Appl. Phys. Lett.*, vol. 99, no. 11, 2011, Art. no. 113517.
[11] J. Huang, T. Wang, L. Hua, J. Fan, H. Xiao, and M. Luo, "A coaxial cable Fabry–Perot interferometer for sensing applications," *Sensors*, vol. 13, no. 11, pp. 15252–15260, 2013.
[12] J. Huang, T. Wei, X. Lan, J. Fan, and H. Xiao, "Coaxial cable Bragg grating sensors for large strain measurement with high accuracy," in *Sensors and Smart Structures Technologies for Civil, Mechanical, and Aerospace Systems 2012*, vol. 8345: Bellingham,WA,USA: International Society for Optics and Photonics, 2012, Art. no. 83452Z.
[13] C. Zhu, Y. Zhuang, Y. Chen, B. Zhang, and J. Huang, "Contactless liquid interface measurement based on a hollow coaxial cable resonator," *Sens. Actuators A Phys.*, vol. 285, pp. 623–627, 2019.
[14] C. Zhu, Y. Zhuang, Y. Chen, and J. Huang, "A liquid-level sensor based on a hollow coaxial cable Fabry–Perot resonator with micrometer resolution," *IEEE Trans. Instrum. Meas.*, no. 99, no. 12, pp. 1–6, Dec. 2018.
[15] C. Zhu, Y. Chen, Y. Zhuang, and J. Huang, "A centimeter-range displacement sensor based on a hollow coaxial cable Fabry–Perot resonator," *IEEE Sens. J.*, vol. 18, no. 11, pp. 4436–4442, Jun. 2018.
[16] C. Zhu, Y. Chen, Y. Zhuang, and J. Huang, "Displacement and strain measurement up to 1000 °C using a hollow coaxial cable Fabry–Perot resonator," *Sensors (Basel, Switzerland)*, vol. 18, no. 5, 2018, Art. no. 1304.
[17] C. Zhu, Y. Zhuang, Y. Chen, and J. Huang, "A hollow coaxial cable Fabry–Pérot resonator for liquid dielectric constant measurement," *Rev. Sci. Instrum.*, vol. 89, no. 4, 2018, Art. no. 045003.
[18] M. Han, Y. Zhang, F. Shen, G. R. Pickrell, and A. Wang, "Signal-processing algorithm for white-light optical fiber extrinsic Fabry–Perot interferometric sensors," *Opt. Lett.*, vol. 29, no. 15, pp. 1736–1738, 2004.
[19] S. Fan, K. Staebell, and D. Misra, "Static analysis of an open-ended coaxial line terminated by layered media," *IEEE Trans. Instrum. Meas.*, vol. 39, no. 2, pp. 435–437, Apr. 1990.
[20] C. Zhu, R. E. Gerald, Y. Chen, and J. Huang, "Probing the theoretical ultimate limit of coaxial cable sensing: measuring nanometer-scale displacements," *IEEE Trans. Microw. Theory Tech.*, vol. 68, no. 2, pp. 816–823, Feb. 2020.
[21] D. M. Pozar, *Microwave Engineering*. Hoboken, NJ, USA: Wiley, 2009.
[22] C. Zhu, R. E. Gerald II, Y. Chen, and J. Huang, "Metal-organic framework portable chemical sensor," *Sensors Actuators B: Chemical*, vol. 321, 2020, Art. no. 128608.
[23] C. Zhu, R. E. Gerald II, and J. Huang, "Microwave interferometer for displacement measurements with theoretical picometer resolution," *IEEE Trans. Microw. Theory Tech.*, to be submitted.

Chen Zhu (Student Member, IEEE) received the B.E. degree in opto-electronics information engineering from the Huazhong University of Science and Technology, Wuhan, China, in 2015. He is currently working toward the Ph.D. degree with the Missouri University of Science and Technology, Missouri, USA. His research interest is focused on the development of optical fiber and coaxial cable-based devices for sensing applications in harsh environments. He was a recipient of the IEEE Instrumentation and Measurement Society Graduate Fellowship Award from 2018 to 2019. He is a Student Member of OSA, the IEEE Instrumentation and Measurement Society, and the IEEE Microwave Theory and Techniques Society.

Rex E. Gerald II received the B.A. degree in chemistry from the University of Chicago (UC) and the conjoint Ph.D. degree in physical chemistry from the University of Illinois, Chicago (UIC) and the Max Planck Institute (MPI), Heidelberg. He is a Research Professor with the Lightwave Technology Laboratory of the Department of Electrical and Computer Engineering, Missouri University of Science and Technology (MS&T). He holds 26 US patents and co-authored more than 50 publications from research investigations conducted at UC, UIC, MPI, Argonne National Laboratory, and MS&T.

Jie Huang (Member, IEEE) is the Director and an Assistant Professor of the Lightwave Technology Laboratory of the Department of Electrical and Computer Engineering with the Missouri University of Science and Technology (MS&T). Dr. Huang has performed research in instrumentation and measurement for more than 10 years. Dr. Huang's research focuses on the development of optical and microwave sensors and instrumentation for applications in energy, intelligent infrastructures, clean-environment, and biomedical sensing. Dr. Huang authored or co-authored over 75 refereed articles, 60 conference papers, a book chapter, and 10 US patent applications (five are issued) all in the arena of advanced sensors.

Authorized licensed use limited to: Missouri University of Science and Technology. Downloaded on May 29,2021 at 22:40:03 UTC from IEEE Xplore. Restrictions apply.